This is a repository copy of *Peierls-Nabarro modeling of dislocations in UO₂*.

**Peierls-Nabarro modelling of dislocations in UO$_2$**

Richard Skelton[a,*] and Andrew M. Walker[b]

[a] Research School of Earth Sciences, Australian National University, Canberra, ACT, 0200, Australia

[b] School of Earth and Environment, University of Leeds, Leeds, LS2 9JT, UK

* Corresponding author: richard.skelton@anu.edu.au

**Abstract**

Under conditions of high stress or low temperature, glide of dislocations plays an important role in the deformation of UO$_2$. In this paper, the Peierls-Nabarro model is used to calculate the core widths and Peierls stresses of ½<110> edge and screw dislocations gliding on {100}, {110}, and {111}. The energy of the inelastic displacement field in the dislocation core is parameterized using generalized stacking fault energies, which are calculated atomistically using interatomic potentials. We use seven different interatomic potential models, representing the variety of different models available for UO$_2$. The different models broadly agree on the relative order of the strengths of the different slip systems, with the 1/2<110>{100} edge dislocation predicted to be the weakest slip system and 1/2<110>{110} the strongest. However, the calculated Peierls stresses depend strongly on the interatomic potential used, with values ranging between 2.7-12.9 GPa for glide of 1/2<110>{100} edge dislocations, 16.4-32.3 GPa for 1/2<110>{110} edge dislocations, and 6.8-13.6 GPa for 1/2<110>{111} edge dislocations. The glide of 1/2<110> screw dislocations in UO$_2$ is also found to depend on the interatomic potential used, with some models predicting similar Peierls stresses for glide on {100} and {111}, while others predict a unique easy glide direction. Comparison with previous fully atomistic calculations show that the Peierls-Nabarro model can

accurately predict dislocation properties in $UO_2$.

**Keywords**

**1. Introduction**

$UO_2$ is a common oxide of uranium, and the primary fuel material for nuclear reactors. Under normal conditions, $UO_2$ adopts the fluorite ($CaF_2$) structure, with the $U^{4+}$ ions arranged in a face centered cubic lattice and eight-fold coordinated by $O^{2-}$. $UO_2$ also occurs naturally as a mineral, known as uraninite or pitchblende. Uraninite is the most abundant uranium bearing mineral, and is an important economic source of uranium. Dislocations, a type of linear topological defect that act as carriers of plastic strain, are produced by interaction with radiation during burn-up [1, 2] and are important for understanding the mechanical properties of $UO_2$, especially at low temperatures. Additionally, due to the substantial distortion of the crystal lattice in the vicinity of a dislocation, they can also serve as hosts for impurity atoms in $UO_2$, including fission products such as Ru [3] and the noble gas Xe [4].

There are four main dislocations observed in $UO_2$, $1/2<110>\{100\}$, $1/2<110>\{110\}$, and $1/2<110>\{111\}$ edge dislocations, and a screw dislocation with Burgers vector $1/2<110>$ [5, 6]. Of these, the $1/2<110>\{100\}$ edge dislocation is the weakest (ie. moves under the application of the lowest resolved shear stress), while the $1/2<110>\{110\}$ is the strongest. Computational studies show that the screw dislocation has the lowest energy, while the $1/2<110>\{110\}$ edge dislocation has the highest energy [7, 8]. Under the action of an applied shear stress, a dislocation can be displaced from its equilibrium position and, if the stress exceeds some critical value (referred to as the Peierls stress, $\sigma_p$), the dislocation may begin to move. The Peierls stress and elasticity tensor

2

together determine dislocation mobility below the athermal limit (the temperature above which dislocation velocities are controlled by dislocation-dislocation interactions rather than the Peierls stress), and can be used to model the critical resolved shear stresses, dislocation velocities, and strain rates for a given slip system, as functions of temperature. At stresses below $\sigma_p$, dislocation glide occurs through the thermally activated nucleation and migration of kink-pairs [9]. The velocity at which a dislocation glides is related to the rate of sustainable kink-pair nucleation, the activation energy of which depends on the elastic constants of the material, and on the Peierls barrier. If the activation energy for sustainable kink-pair nucleation at zero applied stress $\Delta E_0$ is known, the stress dependence of the activation energy is

$$\Delta E(\sigma) = \Delta E_0 \left(1 - \left(\sigma/\sigma_p\right)^p\right)^q \tag{1}$$

where p and q are exponents whose values must be determined by fitting to experimental or simulation data [10].

Despite their importance for modeling dislocation velocities and hence strain rates during glide-controlled creep, the Peierls stresses of the major dislocation slip systems in $UO_2$ remain poorly constrained. However, one previous study has used atomistic simulations to calculate the Peierls barrier (which approximately proportional to $\sigma_p$) of edge dislocations in $UO_2$, whose values have the relative ordering 1/2<110>{100} < 1/2<110>{111} < 1/2<110>{110} [7]. High-temperature molecular dynamics calculations of critical shear stresses show that the Peierls stresses of the edge dislocations in $UO_2$ follow the same relative ordering seen in [7], and indicate $\sigma_p$ is at least several GPa for all three slip systems [11]. Atomistic simulations have also shown that glide of 1/2<110>{100} edge dislocations occurs via a thermally activated mechanism below 2000 K, which is consistent with a relatively high (>1 GPa) Peierls stress for this slip system [12]. Hyper-stoichiometry is known to affect the slip systems of $UO_2$, reducing the critical resolved shear stress

3

[6, 13]. The magnitude of this effect is greater on the {111} slip plane than on the {100} slip plane [6], causing their critical resolved shear stresses to converge at high temperature and oxygen fugacity.

Peierls stresses can be calculated directly using atomistic methods, either by applying a stress/strain to a supercell and determining the stress required to move the dislocations or by calculating the energies of structures intermediate between adjacent dislocation energies, giving an energy profile whose derivative is proportional to the Peierls stress. A simpler alternative to the fully atomistic approach is the Peierls-Nabarro (PN) model, which uses a hybrid continuum-atomistic approach to model dislocations. In the PN model, a dislocation is represented as a finite distribution of partial dislocations, whose elastic interactions are balanced by some inelastic restoring force [14, 15]. Atomistic simulation methods can be used to parameterize this force by introducing a generalized stacking fault (GSF) into a simulation cell, which is done by displacing one half of the cell with respect to the other [16]. One clear advantage of the PN model over fully atomistic simulations is that the bulk of the computational cost is incurred in the generalized stacking fault (GSF) calculations used to parameterize the inelastic forces. As these contain far fewer atoms than are found in the simulation cells used to perform fully atomistic calculations of dislocation properties, the PN method can be used to calculate dislocation widths and Peierls stresses far more quickly and at lower computational cost than is possible with fully atomistic calculations.

The Peierls stress is an important parameter governing glide mobility of dislocations, knowledge of which is essential to accurately model glide-controlled creep processes during, for example, burn-up of $UO_2$. In this study, we use the Peierls-Nabarro model to calculate the dislocation misfit profiles and Peierls stress for the most important slip systems in $UO_2$ To do this, we first calculate the γ-surfaces (ie. GSF energies over a range of different stacking fault vectors) corresponding to the main slip systems, using seven different interatomic potentials for $UO_2$. This subset of potentials

was chosen to cover the range of possible parameterizations available in the literature and typically used to model $UO_2$. The models include full- and partial-charge models, rigid ions, shell models, and a recent many-body model, and allow us to infer the general behavior of these classes of parameterizations for modeling dislocations in $UO_2$. From the Peierls-Nabarro model, we are then able to use these γ-surfaces to calculate misfit profiles and Peierls stresses for the 1/2<110>{100}, 1/2<110>{110}, and 1/2<110>{111} edge dislocations and the 1/2<110>{110} screw dislocations in $UO_2$. In addition to providing intrinsic dislocation properties, allowing us to compare the suitability of different interatomic potentials for dislocation modeling, and evaluate the viability of using the PN method to study dislocations in $UO_2$.

## 2. Computational Methods

### 2.1 The Peierls-Nabarro Model

In the Peierls-Nabarro (PN) model, a dislocation with finite core-width is represented as a distribution of partial dislocations along the glide plane, whose shape is determined by the balance between the elastic energies acting between its constituent partial dislocations and the inelastic energy introduced by the presence of a disregistry **u** in the material at the glide plane, with the former acting to broaden the dislocation distribution and the latter serving to constrain it. The PN model, as used in this study, is briefly summarized below. For a more complete treatment, see Bulatov and Cai [17].

The value of the total energy of such a finite distribution of dislocations at a distance $R$ from the dislocation line is

$$E_{TOT}(R) = E_{ELASTIC} + E_{MISFIT} + Kb^2 lnR \qquad (2)$$

where $K$ is an energy prefactor whose value depends on the elastic constants and the dislocation

orientation, and $b$ is the Burgers vector magnitude. $E_{ELASTIC}$ is the elastic interaction energy between the partials, $E_{MISFIT}$ the energy due to the inelastic displacement of atoms at the glide plane, and final term gives the strain energy due to the long-ranged elastic strain field of the dislocation. As the long-ranged term is independent of the core structure and $E_{WORK}$ is zero in the absence of an applied stress, the solution to PN model is the dislocation distribution that to minimizes the energy function

$$E_{INTERNAL} = E_{ELASTIC} + E_{MISFIT} \qquad (3)$$

If $\mathbf{u}(x)$ is the disregistry across the slip plane and $\rho(x) = du_i(x)/dx$ is the associated dislocation density distribution, then the elastic energy of the dislocation is the work required to insert this disregistry into an infinite elastic medium:

$$E_{ELASTIC}[\rho(x)] = - K \iint \rho(x')\rho(x)dx'dx \qquad (4)$$

It is worth noting that the effect of the elastic energy is to cause the dislocation to spread out so that, if there were no restoring force, the dislocation density distribution would be zero everywhere (but with finite integral). In real crystals, it is the energy penalty associated with introducing misfit on either side of the slip plane that provides this opposing force, and constrains dislocations to have finite width. For a given disregistry profile $\mathbf{u}(x)$, the inelastic energy is

$$E_{MISFIT} = \sum_n \gamma\left(u(na_p)\right)a_p \qquad (5)$$

where $a_p$ is the spacing between adjacent atomic planes and $\gamma$, called a $\gamma$-line in one dimension and the $\gamma$-surface in two, is a function that gives the energy required to displace one half of a crystal with respect to the other by $\mathbf{u}$ [16]. The misfit energy can also be written as an integral, in which case the dislocation energy is invariant under translation, implying that the dislocation is mobile

under the application of an infinitesimal external stress. When calculating the dislocation core structure numerically, the misfit profiles is expanded as a sum of arctangent functions (ie. partial dislocations), as

$$u(x) = \frac{b}{\pi} \sum_i A_i \arctan\left(\frac{x - x_{0,i}}{c_i}\right) - C$$  (6)

where C is *b/2* for the component of misfit parallel to the Burgers vector and zero otherwise. The parameters $x_{0,i}$, $A_i$, and $c_i$ are found by minimizing equation (3), with the elastic and misfit terms represented by equations (4) and (5), respectively, with the disregistry function given in the form of equation (6).

The evolution of the disregistry profile under the action of an applied stress σ is computed by adding $E_{WORK} = \sigma \int u(x)\, dx$ to the total internal energy (equation 3) of the dislocation and minimising the energy functional as before. At the Peierls stress, $\sigma_p$, the energy barrier inhibiting free translation of the dislocation disappears, allowing it to glide indefinitely.

There are two key assumptions in the PN model as given in the preceding discussion. The first is that non-linear interactions between adjacent partial dislocations in the dislocation density distribution $\rho(x)$ are negligible, so that equation (5) can be written as a linear sum of GSF energies, and this is generally true. The second assumption is that the dislocation core structure is planar, and localized on the glide plane. This is generally correct in the case of pure edge dislocations, but may fail for some screw dislocations if they spread on multiple glide planes, as is the case for [001] screw dislocations in forsterite [18], which glide via a locking-unlocking mechanism [19]. If a screw dislocation exhibits non-planar core-spreading, the PN model still provides a lower bound on the Peierls stress, as dislocations with planar cores are more mobile than those with non-planar

cores.

*2.2 Generalized stacking fault calculations*

The γ-surface energy used to calculate the inelastic energy of a dislocation density distribution is constructed from generalized stacking fault (GSF) energies obtained from atomistic calculations. This is done for each slip system by taking an appropriately oriented supercell of $UO_2$ and displacing the top half of the construction simulation cell along a grid of stacking fault vectors and relaxing the atomic coordinates, subject to the constraint that both U and O can only relax perpendicular to the slip plane. The excess energy of the slipped cell is obtained by comparing the energy of the undeformed crystal with that of the fully relaxed supercell. As the simulation cell is 3D periodic, this construction actually inserts a pair of equivalent stacking faults into the cell (at z=0 and z=0.5), so that the GSF energy is 1/2 the calculated excess energy of the deformed supercell.

The dependence of the generalized stacking fault energies on the simulation cell thickness (perpendicular to the slip plane) was tested for each lattice orientation. For {100} and {111} slip planes, atomic slabs 10 unit cells thick were sufficient to converge the calculated 1/4<110> stacking fault energies on each surface to within < 2%, while for the {110} slip plane, the fully converged simulation cell was 14 unit cells. These simulation cells are displayed in Fig. 1.

In this study, seven different interatomic potentials are used to calculate the properties of dislocations in $UO_2$. In addition to the highly-accurate embedded atom potential developed by Cooper et al. [20], we use the Arima potential [21], which is a rigid-ion model that treats all interatomic interactions using the Buckingham potential, and the Goel potential [22], which is similar to the potential developed by Arima et al., but treats the polarizability of the O ions using a shell model [23]. Additionally, we use the Morelon potential [24], which simulates the O-O

interactions with a Buckingham 4-range potential, and has previously been used by Parfitt et al. [7] to study dislocation motion atomistically, and the potentials developed by Basak et al. [25] and Yakub et al. [26, 27], which are rigid ion models, including Morse terms to simulate the covalent part of U-O pair interactions. Finally, we also use the Read potential, in which a Buckingham 4-range potential is used to model the O-O interactions and includes shells for the O ions [28]. Both the Arima and Read potentials take the charges on the U and O atoms to be equal to their formal charges, while the other five potentials are partially ionic. For convenience, these potentials will be referred to henceforth as Arima05, Basak03, Cooper14, Goel08, Morelon03, Read10, and Yakub10. All atomistic calculations of GSF energies are performed using the molecular mechanics code GULP [29, 30].

## 3. Results and discussion

The {100}, {110}, and {111} γ-surfaces calculated using the seven interatomic potentials are displayed in Fig. 2, with the important stable and unstable stacking fault energies listed in Table 1. Note that the shape of the {111} gamma surface presented here differs from that in [11] because there are two non-equivalent heights at which the slip plane may intersect the simulation cell, either separating a layer of U atoms and a layer of O atoms, or two adjacent layers of O atoms. Here, the latter choice is used as it gives lower generalized stacking fault energies and a simpler γ-surface shape, whereas Fossati et al. appear to have placed the slip plane between the U and O layers. These layers are closely spaced, such that atoms sometimes pass close to one another, resulting in an irregular γ-surface characterized by high maximum GSF energies.

As can be seen from Fig. 2, the seven potentials can be separated into two broad groups based on the shape of the {100} γ-surface. In the first group, which comprises Arima05, Goel08, Morelon03, and Read10, the 1/4<110> generalized stacking fault corresponds to a saddle point of the γ-surface.

In contrast, this stacking fault vector is associated with a local maximum of the γ-surface energy for the Basak03, Cooper14, and Yakub10 potentials. Furthermore, this group of potentials all show a local minimum along <100>, which is deepest for the Cooper14 potential and shallowest for the Basak03 potential. Despite the disparity in the shapes of the γ-surfaces calculated using the different potentials, the 1/2<110>{100}, 1/2<110>{110}, and 1/2<110>{111} γ-lines remain qualitatively similar (see Fig. 3), although the range of stacking fault maxima predicted for each line is quite large. The shape of these γ-lines will largely determine the properties of their associated slip systems, indicating that the qualitative features predicted for the major slip systems in $UO_2$ are likely to be similar for all seven potential models, although the dislocation widths and Peierls stresses may vary greatly.

From these γ-surfaces, dislocation misfit profiles were calculated for the three types of edge dislocation and 1/2<110> screw dislocations gliding on {100}, {110}, and {111}. Although we performed all calculations using the 2D Peierls Nabarro model, no spreading perpendicular to **b** was found for any of the slip systems (ie. for all *i* corresponding to the perpendicular component). This means that the three edge dislocations are not predicted to have a screw component, while the 1/2<110> screw dislocation has no edge component. For consistency between the static structures and Peierls stresses, the misfit energy has been calculated using a sum over discrete lattice planes rather than the integral formulation. For the edge dislocations, the interlayer spacing is *b*, the Burgers vector thickness. For 1/2<110> screw dislocations gliding on {100}, the interlayer spacing is likewise *b*, while for screw dislocations spreading on {110} or {111}, the interlayer spacing is a/2 (where *a* is the lattice parameter) and $b\sqrt{2}/2$, respectively. Calculated dislocation widths and dislocation energies are listed in Table 2 for all of the potentials, while representative disregistry profiles and their associated dislocation density distributions (obtained using the Cooper14 potential) are plotted in Fig. 4.

One of the key parameters defining a dislocation core is the core width, defined as distance over which the disregistry field changes from -**b**/4 to **b**/4. For all potentials examined in this study, the 1/2<110>{100} edge dislocation had the widest core and the <110>{110} screw dislocation the narrowest. The Arima05, Goel08, and Morelon03 potentials had unusually narrow 1/2<110>{100} and 1/2<110>{111} edge dislocations, while the Basak03 potential predicted an unusually wide core for the 1/2<110>{100} edge dislocation, compared with the other potentials. Predictions for the shape of the 1/2<110>{111} misfit profile were particularly consistent between the different potentials, with a minimum width of 2.471 Å (Basak03) and a maximum width of 2.776 Å (Morelon03). The shapes of the 1/2<110>{110} edge and screw dislocations were remarkably consistent between the seven potentials. As can be seen in Table 2 and Fig 4d, the 1/2<110> screw dislocations has a particularly narrow core, and the widths of screw dislocations spreading on {110} and {111} are considerably less than that of a screw dislocation spreading on {100}. This indicates that the 1/2<110> screw dislocation is essentially planar, and that its Peierls stress can thus be calculated using the PN method.

While the ordering of the energies for the three edge dislocations considered here agree with the fully atomistic calculations of Murphy et al. [8], we find that the 1/2<110>{100} edge dislocation has a lower energy than a 1/2<110> screw dislocation spreading on {100}, whereas they reported that screw dislocations have the lowest line energy. However, this disparity can be attributed to the fact that Murphy et al. report the relative ordering of the dislocation energies at a distance 40 Å from the dislocation line. In atomistic simulations, the dislocation energy as a function of radius is

$E_{TOT} = E_{CORE} + Kb^2 \ln(R/R_{core})$ . At large distances from the dislocation line, the total energy is dominated by the second term, which is the elastic energy of the dislocation strain field. Since the energy coefficient $K$ for a screw dislocation is necessarily lower than that of an edge dislocation (for an isotropic material, $K_{edge} = K_{screw}/(1-\nu)$, where $\nu > 0$ is the Poisson's ratio) the energy of a screw

dislocation at a distance of 40 Å from the dislocation line (the distance at which Murphy et al. calculated dislocation line energy) will usually be lower than that of an edge dislocation with the same magnitude Burgers vector.

Perhaps more relevant are the core (ie. inelastic) energies obtained by Parfitt et al. [7], where the order of the calculated core energies is $E_{<110>\{110\}} > E_{<110>\{111\}} > E_{<110>\{100\}}$, a result identical to that found for five of the seven potentials in this study. The exceptions are the Morelon03 and Read10 potentials, with the former predicting that the 1/2<110>{111} is the lowest energy dislocation, whereas the latter actually predicts that the 1/2<110>{100} dislocation has the highest energy of the three major slip systems. Contrary to the atomistic calculations in [8], the PN model predicts that 1/2<110> screw dislocations in $UO_2$ have higher core energies than any of the 1/2<110> edge dislocations. However, this discrepancy may be attributed to the presence of the elastic energy term, as Parfitt et al. use a cutoff radius of 30 Å to fit the core energy, and the trade-off between the parameters $E_{CORE}$ and $R_{CORE}$ mean that their reported core energy will contain a substantial contribution from elastic strain energy of the region $R < R_{CORE}$.

Peierls stresses are calculated using the applied stress method for all three edge dislocation slip systems, and for 1/2<110> screw dislocations gliding on {100}, {110}, and {111}. The values calculated are listed in Table 3. For all seven potentials, slip on the {110} plane is associated with the highest Peierls stresses, consistent with experimental observations of relative slip system strengths, with predicted stresses for glide of the edge dislocation in this direction as great as 32.3 GPa (Arima05), although the other six potentials predict somewhat lower values (16.4-22.9 GPa). Of the potential models used in this study, six predict that the 1/2<110>{100} slip is weakest, as has been found in experiments. The lone exception is the Read10 potential, for which the 1/2<110>{100} edge dislocation has a Peierls stress of 12.9 GPa, compared with a $\sigma_p$ of 8.1 GPa for glide of the 1/2<110>{111} edge dislocation. Comparing calculated Peierls stresses for Read10

with those of the other six potential, it appears that the specific problem is that Read10 overestimates the strength of the 1/2<110>{100} slip systems, as the calculated Peierls stresses for dislocation glide on {110} and {111} are broadly similar to those obtained with other potentials. While the Morelon03 potential still predicts that 1/2<110>{100} will be softer than 1/2<110>{111}, the contrast is much less than for the other potentials.

For screw dislocations, the line vector $\xi$ and Burgers vector **b** are parallel. Consequently, screw dislocations can glide on any plane whose normal is perpendicular to **b**. For the 1/2<110> screw dislocation in $UO_2$, possible glide planes include {100}, {110}, and {111}, and the calculated Peierls stresses for these possible slip systems are presented in Table 3. As can be seen, the relative ease of screw dislocation glide on the different planes is strongly dependent on the interatomic potential used. The Basak03 and Yakub10 potentials both predict that 1/2<110> screw dislocations glide most easily on {100}, while glide is most difficult on {110}. The calculated value of $\sigma_p$ for glide on {111} is intermediate between the two. This is also the case for calculations performed using the Cooper14 potential, although in this case the Peierls stresses for glide on {100} and {111} are more similar. While the Arima05, Goel08, and Morelon03 potentials find that {110} glide has the highest Peierls stress, all three give almost identical Peierls stresses for glide on {100} and {111}. For the Arima05, Cooper14, Goel08, and Morelon03 potentials, the similarity of the Peierls stresses for slip on {100} and {111} suggests that cross-slip between these planes should be possible. Finally, as is the case for the edge dislocation slip systems, the Read10 potential predicts substantially different relative ordering of the Peierls stresses, with the Peierls stress for glide on {111} (11.1 GPa) is lower than those for glide on {100} or {110}, for which the calculated values of $\sigma_p$ are 16.2 and 16.7 GPa, respectively.

There is no apparent systematic variation in the Peierls stress with the oxygen polarisability, except

that shell models predict marginally a lower value for the Peierls barrier of the 1/2<110>{111} edge dislocation. However, the difference is no larger than the variation seen within the rigid models. Similarly, there is no systematic difference between models with formal charges and those that use partial ionic charges. From this, we conclude that variations between the different models are a consequence of the values of the fitted parameters, rather than the style of model used.

While, of the seven potentials considered in this study, for only one (Read10) are the calculated values of $\sigma_p$ inconsistent with the known relative strengths of the {100}, {110}, and {111} glide planes, the scatter in the calculated values is quite high. Below the athermal limit, the activation energy for glide creep is given by the expression for the critical energy for sustainable kink-pair nucleation (equation (1)). This depends on the value of $\sigma_p$ which, as has been shown, depends on the choice of potential. Indeed, since dislocation velocities and strain rates have an Arrhenius relationship to the activation energy, high temperature simulations of glide-controlled creep will be more sensitive to the choice of potential than might be expected judging from the Peierls stresses alone. This means that future attempts to model deformation via glide-controlled mechanism will have to be careful in interpreting their results, as these will depend on the potential used.

The Peierls potential is the energy barrier separating adjacent minima of the dislocation. For undissociated dislocations, the approximate shape of the Peierls potential may be calculated from the Peierls stress and Burgers vector magnitude as

$$W_P(X) = \frac{\sigma_p b^2}{2\pi}\left[1 - \cos\left(\frac{2\pi x}{b}\right)\right] \tag{5}$$

It follows that the maximum height of the Peierls potential (also called the Peierls barrier) is simply

$W_{p,max} = \frac{\sigma_p b^2}{\pi}$ . For the Morelon03 potential, using the Peierls stresses from Table 3 and the

Burgers vector magnitude $b$ = 3.852 Å, the Peierls barriers for glide on 1/2<110>{100}, 1/2<110>{110}, and 1/2<110>{111} edge dislocations are 0.17 eV/Å, 0.50 eV/Å, and 0.25 eV/Å, respectively. For comparison, Parfitt et al. [7] used fully atomistic calculations (with interatomic interactions treated using the Morelon03) potential, together with the nudged elastic band (NEB) method to directly calculate Peierls barriers for the three edge dislocations, obtaining values of 0.25 eV/Å, 0.46 eV/Å and 0.31 eV/Å for 1/2<110>{100}, 1/2<110>{110}, and 1/2<110>{111} edge dislocation. The value for the Peierls barrier of the 1/2<110>{110} slip system is well reproduced by the PN model. In contrast, the 1/2<110>{100} and 1/2<110>{111} slip systems are moderately lower than those found by Parfitt et al, which may be because slip paths found in their NEB calculations do not correspond to the global minimum energy pathways or a consequence of the relatively short cut-off (25 Å) used in their simulations, which may have allowed the dislocations to interact with the boundary of the simulation cell, creating an artificial barrier to glide. Alternatively, the difference may indicate the presence of non-planar dislocation core spreading in the atomistic calculations which, as previously discussed, would result in higher Peierls stresses than those found for the labile planar dislocations produced by PN modeling. Nevertheless, it should be noted that the Peierls barriers calculated using the PN model are of the same order of magnitude as those found by Parfitt et al. [7], and that both methods predict the same order for the slip system strengths.

The close comparison between the results presented here and fully atomistic calculations suggest that the PN model can be used to accurately model the mobility of dislocations in $UO_2$. However, previous studies of dislocation glide [7, 11, 12] used the same potential (Morelon03) to model interatomic interactions. Murphy et al [8] compared $UO_2$ dislocation core structures predicted by a range of different potentials, and found that several of them produced highly disordered dislocation core structures, with a substantially non-planar character. As discussed in the methods section, the

particular formulation of the PN model used here is applicable only to dislocations with a planar core, as it assumes that the disregistry field is localized on the glide plane. However, the disordered cores found for some of the potentials are likely a consequence of the fact that the input displacement fields were derived from classical elasticity theory, leading to high stresses near the dislocation line (especially for the $1/2<110>\{110\}$ edge dislocation), and substantial forces on some of the individual atoms. Given the large number of degrees of freedom available in a fully atomistic calculation, it is plausible that the non-compact, disordered core structures found in [8] for some of the potentials actually reflects relaxation of the dislocation into a local energy minimum. That this might be the case is supported by the fact that the core width predicted for each dislocation is relatively consistent across the seven potentials, with the greatest spread (~1 Å) seen for the $1/2<110>\{100\}$ edge dislocation. Moreover, all of the potentials predict that the $1/2<110>$ screw dislocation and the $1/2<110>\{100\}$, $1/2<110>\{110\}$, and $1/2<110>\{111\}$ edge dislocations in $UO_2$ have narrow cores, with no apparent splitting into partial dislocations.

In this study, we have focused on dislocations moving in point defect-free $UO_2$. However, the PN method of modeling dislocation glide also allows the effect of point defect-dislocation interactions on the Peierls stress of a dislocation to be calculated straightforwardly. To do this, point defect of the desired type are inserted at or near the slip planes in generalized stacking fault calculations, whose energies are processed to produce the g-line/surface which enters the expression for the inelastic misfit energy (equation (5)) in a PN model. This approach has been used previously to help explain the mechanisms by which interstitial hydrogen atoms [31] and lattice vacancies [32] lubricate dislocation glide in fcc Al. The PN model has also been used to show that Sn alloying reduces the Peierls stress of basal dislocations in Zircaloy, relative to pure Zr [33], and that alloying with Yt similarly enhances basal glide in Mg metal [34]. In $UO_2$, oxygen hyper-stoichiometry (ie. O/U > 2) reduces the measured critical resolved shear stress, and changes the relative strengths of

the 1/2<110>{100} and 1/2<110>{111} slip systems by enhancing the mobility of the latter [6, 13]. The precise mechanism by which this occurs is unclear, but one possibility is that the presence of oxygen defects incorporated at interstitial sites reduces the Peierls stress [35]. Since the PN method can be used to calculate $\sigma_p$ for the major edge dislocation slip systems in stoichiometric $UO_2$ returning values comparable to those calculated from atomistic simulations, it is likely that the PN will also be can also be applied to dislocation glide in hyper-stoichiometric $UO_{2+x}$.

## 4. Conclusions

Using several commonly used interatomic potential models, we studied the structures and mobilities of the major dislocation slip systems found in $UO_2$ using the Peierls-Nabarro model parameterised with generalized stacking fault energies obtained from atomistic calculations. It was found that all three edge dislocations have no screw component, and that the screw dislocation had no edge component. For all seven potentials, the 1/2<110>{110} edge and screw dislocations had the highest core energies. For the Read10 and Morelon03 potentials, it was found that the calculated core energies for 1/2<110>{111} edge dislocations exceed those of the 1/2<110>{100} edge dislocations, contradicting the results for the other five potentials as well as previous computational studies[7, 8].

Of the seven potential models considered here, only Read10 fails to correctly identify the 1/2<110>{100} slip system as having the lowest Peierls stress. Looking at the other six potentials, we found that the Peierls stresses are strongly dependent on the model used with, for instance, $\sigma_p$ for the dominant 1/2<110>{100} slip system varying from as little as 2.7 GPa (Basak03) to as much as 5.8 GPa (Morelon03). However, all six predict that the order of the dislocation slip systems, from weakest to strongest, is 1/2<110>{100} < 1/2<110>{110} < 1/2<110>{111}, consistent with both experiments [5, 6] and fully atomistic calculations [7, 11] showing that, where suitable potentials

are available, the Peierls-Nabarro approach can be used to predict dislocation properties in $UO_2$. Unfortunately, since there are no experimental measurements or *ab initio* calculations of Peierls stresses for individual dislocation slip systems in $UO_2$, it is presently impossible to determine which of the potentials considered here is best suited for modeling dislocations in $UO_2$.

**Acknowledgements**

**References**

[1]

K. Nogita, K. Une, Irradiation-induced recrystallization in high burnup UO2 fuel, Journal of Nuclear Materials. 226 (1995) 302–310. doi:10.1016/0022-3115(95)00123-9.

[2]

V.G. Baranov, A.V. Lunev, A.V. Tenishev, A.V. Khlunov, Interaction of dislocations in UO2 during high burn-up structure formation, Journal of Nuclear Materials. 444 (2014) 129–137. doi:10.1016/j.jnucmat.2013.09.042.

[3]

A. Goyal, T. Rudzik, B. Deng, M. Hong, A. Chernatynskiy, S.B. Sinnott, S.R. Phillpot, Segregation of ruthenium to edge dislocations in uranium dioxide, Journal of Nuclear Materials. 441 (2013) 96–

102. doi:10.1016/j.jnucmat.2013.05.031.

[4]

P.V. Nerikar, D.C. Parfitt, L.A. Casillas Trujillo, D.A. Andersson, C. Unal, S.B. Sinnott, R.W. Grimes, B.P. Uberuaga, C.R. Stanek, Segregation of xenon to dislocations and grain boundaries in uranium dioxide, Phys. Rev. B. 84 (2011) 174105. doi:10.1103/PhysRevB.84.174105.

[5]

K.H.G. Ashbee, C.S. Yust, A mechanism for the ease of slip in UO2+x, Journal of Nuclear Materials. 110 (1982) 246–250. doi:10.1016/0022-3115(82)90152-0.

[6]

R.J. Keller, T.E. Mitchell, A.H. Heuer, Plastic deformation in nonstoichiometric UO2 + x single crystals—II. Deformation at high temperatures, Acta Metallurgica. 36 (1988) 1073–1083. doi:10.1016/0001-6160(88)90161-7.

[7]

D.C. Parfitt, C.L. Bishop, M.R. Wenman, R.W. Grimes, Strain fields and line energies of dislocations in uranium dioxide, J. Phys.: Condens. Matter. 22 (2010) 175004. doi:10.1088/0953-8984/22/17/175004.

[8]

S.T. Murphy, M.J.D. Rushton, R.W. Grimes, A comparison of empirical potential models for the simulation of dislocations in uranium dioxide, Progress in Nuclear Energy. 72 (2014) 27–32. doi:10.1016/j.pnucene.2013.09.010.

[9]

H. Koizumi, H.O.K. Kirchner, T. Suzuki, Kink pair nucleation and critical shear stress, Acta Metallurgica et Materialia. 41 (1993) 3483–3493. doi:10.1016/0956-7151(93)90228-K.

[10]

U.F. Kocks, A.S. Argon, M.F. Ashby, Thermodynamics and kinetics of slip, Pergamon Press, Oxford, 1975.

[11]

P. Fossati, L. Van Brutzel, B. Devincre, Molecular dynamics simulation of dislocations in uranium dioxide, Journal of Nuclear Materials. 443 (2013) 359–365. doi:10.1016/j.jnucmat.2013.07.059.

[12]

A.V. Lunev, A.Y. Kuksin, S.V. Starikov, Glide mobility of the 1/2[1 1 0](0 0 1) edge dislocation in UO2 from molecular dynamics simulation, International Journal of Plasticity. 89 (2017) 85–95. doi:10.1016/j.ijplas.2016.11.004.

[13]

C.S. Yust, C.J. McHARGUE, Deformation of Hyperstoichiometric UO2 Single Crystals, Journal of the American Ceramic Society. 54 (1971) 628–635. doi:10.1111/j.1151-2916.1971.tb16019.x.

[14]

R. Peierls, The size of a dislocation, Proc. Phys. Soc. 52 (1940) 34. doi:10.1088/0959-5309/52/1/305.

[15]

F.R.N. Nabarro, Dislocations in a simple cubic lattice, Proc. Phys. Soc. 59 (1947) 256.

doi:10.1088/0959-5309/59/2/309.

[16]

J.W. Christian, V. Vítek, Dislocations and stacking faults, Rep. Prog. Phys. 33 (1970) 307.

doi:10.1088/0034-4885/33/1/307.

[17]

V. Bulatov, W. Cai, Computer Simulations of Dislocations, Oxford Series on

Material Modelling, Oxford University Press, 2006.

[18]

P. Carrez, A.M. Walker, A. Metsue, P. Cordier, Evidence from numerical modelling for 3D

spreading of [001] screw dislocations in Mg2SiO4 forsterite, Philosophical Magazine. 88 (2008)

2477–2485. doi:10.1080/14786430802363804.

[19]

F.R.N. Nabarro, Fifty-year study of the Peierls-Nabarro stress, Materials Science and Engineering:

A. 234 (1997) 67–76. doi:10.1016/S0921-5093(97)00184-6.

[20]

M.W.D. Cooper, M.J.D. Rushton, R.W. Grimes, A many-body potential approach to modelling the

thermomechanical properties of actinide oxides, J. Phys.: Condens. Matter. 26 (2014) 105401. doi:10.1088/0953-8984/26/10/105401.

[21]

T. Arima, S. Yamasaki, Y. Inagaki, K. Idemitsu, Evaluation of thermal properties of UO2 and PuO2 by equilibrium molecular dynamics simulations from 300 to 2000 K, Journal of Alloys and Compounds. 400 (2005) 43–50. doi:10.1016/j.jallcom.2005.04.003.

[22]

P. Goel, N. Choudhury, S.L. Chaplot, Atomistic modeling of the vibrational and thermodynamic properties of uranium dioxide, UO2, Journal of Nuclear Materials. 377 (2008) 438–443. doi:10.1016/j.jnucmat.2008.03.020.

[23]

B.G. Dick, A.W. Overhauser, Theory of the Dielectric Constants of Alkali Halide Crystals, Phys. Rev. 112 (1958) 90–103. doi:10.1103/PhysRev.112.90.

[24]

N.-D. Morelon, D. Ghaleb, J.-M. Delaye, L. Van Brutzel, A new empirical potential for simulating the formation of defects and their mobility in uranium dioxide, Philosophical Magazine. 83 (2003) 1533–1555. doi:10.1080/1478643031000091454.

[25]

C.B. Basak, A.K. Sengupta, H.S. Kamath, Classical molecular dynamics simulation of UO2 to predict thermophysical properties, Journal of Alloys and Compounds. 360 (2003) 210–216.

doi:10.1016/S0925-8388(03)00350-5.

[26]

E. Yakub, C. Ronchi, D. Staicu, Diffusion of helium in non-stoichiometric uranium dioxide, Journal of Nuclear Materials. 400 (2010) 189–195. doi:10.1016/j.jnucmat.2010.03.002.

[27]

E. Yakub, C. Ronchi, D. Staicu, Computer simulation of defects formation and equilibrium in non-stoichiometric uranium dioxide, Journal of Nuclear Materials. 389 (2009) 119–126. doi:10.1016/j.jnucmat.2009.01.029.

[28]

M.S.D. Read, R.A. Jackson, Derivation of enhanced potentials for uranium dioxide and the calculation of lattice and intrinsic defect properties, Journal of Nuclear Materials. 406 (2010) 293–303. doi:10.1016/j.jnucmat.2010.08.044.

[29]

J.D. Gale, GULP: A computer program for the symmetry-adapted simulation of solids, J. Chem. Soc., Faraday Trans. 93 (1997) 629–637. doi:10.1039/A606455H.

[30]

J.D. Gale, A.L. Rohl, The General Utility Lattice Program (GULP), Molecular Simulation. 29 (2003) 291–341. doi:10.1080/0892702031000104887.

[31]

G. Lu, Q. Zhang, N. Kioussis, E. Kaxiras, Hydrogen-Enhanced Local Plasticity in Aluminum: An Ab Initio Study, Phys. Rev. Lett. 87 (2001) 95501. doi:10.1103/PhysRevLett.87.095501.

[32]

G. Lu, E. Kaxiras, Can Vacancies Lubricate Dislocation Motion in Aluminum?, Phys. Rev. Lett. 89 (2002) 105501. doi:10.1103/PhysRevLett.89.105501.

[33]

Y. Udagawa, M. Yamaguchi, T. Tsuru, H. Abe, N. Sekimura, Effect of Sn and Nb on generalized stacking fault energy surfaces in zirconium and gamma hydride habit planes, Philosophical Magazine. 91 (2011) 1665–1678. doi:10.1080/14786435.2010.543651.

[34]

T. Tsuru, Y. Udagawa, M. Yamaguchi, M. Itakura, H. Kaburaki, Y. Kaji, Solution softening in magnesium alloys: the effect of solid solutions on the dislocation core structure and nonbasal slip, J. Phys.: Condens. Matter. 25 (2013) 22202. doi:10.1088/0953-8984/25/2/022202.

[35]

J.S. Nadeau, Dependence of Flow Stress on Nonstoichiometry in Oxygen-Rich Uranium Dioxide at High Temperatures, Journal of the American Ceramic Society. 52 (1969) 1–7. doi:10.1111/j.1151-2916.1968.tb11863.x-i1.

**Tables**

| | 1/4<110>{100} | 1/4<110>{110} | 1/4<110>{111} |
|---|---|---|---|
| | (eV/Å²) | (eV/Å²) | (eV/Å²) |
| Arima05 | 0.2121 | 0.3754 | 0.2252 |
| Basak03 | 0.1202 | 0.2701 | 0.1760 |
| Cooper14 | 0.1522 | 0.2477 | 0.1620 |
| Goel08 | 0.1358 | 0.2434 | 0.1445 |
| Morelon03 | 0.1410 | 0.2156 | 0.1224 |
| Read10 | 0.2090 | 0.2327 | 0.1598 |
| Yakub10 | 0.1300 | 0.2372 | 0.1533 |

**Table 1** Key generalized stacking fault energies, in for the {100}, {110}, and {111} planes

| Slip system | | Arima05 | Basak03 | Cooper14 | Goel08 | Morelon03 | Read10 | Yakub10 |
|---|---|---|---|---|---|---|---|---|
| 1/2<110>{100} edge | ξ (Å) | 2.926 | 3.552 | 2.932 | 3.090 | 2.776 | 2.478 | 2.929 |
| | E (eV/Å²) | -0.472 | -0.385 | -0.298 | -0.405 | -0.227 | -0.152 | -0.269 |
| 1/2<110>{100} screw | ξ (Å) | 2.772 | 3.089 | 2.624 | 2.935 | 2.468 | 2.323 | 2.697 |
| | E (eV/Å²) | -0.307 | -0.268 | -0.143 | -0.282 | -0.089 | -0.062 | -0.168 |
| 1/2<110>{110} edge | ξ (Å) | 2.310 | 2.317 | 2.469 | 2.472 | 2.468 | 2.478 | 2.466 |
| | E (eV/Å²) | -0.154 | -0.097 | -0.158 | -0.140 | -0.140 | -0.196 | -0.137 |
| 1/2<110>{110} screw | ξ (Å) | 1.694 | 1.699 | 1.698 | 1.699 | 1.774 | 1.781 | 2.158 |
| | E (eV/Å²) | 0.216 | 0.172 | 0.39 | 0.137 | 0.089 | 0.099 | 0.132 |
| 1/2<110>{111} edge | ξ (Å) | 2.618 | 2.471 | 2.624 | 2.626 | 2.776 | 2.633 | 2.620 |
| | E (eV/Å²) | -0.301 | -0.184 | -0.233 | -0.221 | -0.282 | -0.250 | -0.209 |
| 1/2<110>{111} screw | ξ (Å) | 2.156 | 2.085 | 2.161 | 2.163 | 2.237 | 2.168 | 2.158 |
| | E (eV/Å²) | -0.052 | -0.015 | -0.033 | -0.043 | -0.088 | -0.042 | -0.029 |

**Table 2** Dislocation core widths (ξ) and core energies calculated from each potential model

| Potential | 1/2<110>{100} | | 1/2<110>{110} | | 1/2<110>{111} | |
|---|---|---|---|---|---|---|
| | edge | screw | edge | screw | edge | screw |
| Arima05 | 3.4(1) | 10.6(1) | 32.3(0) | 31.0(2) | 11.2(1) | 13.9(2) |
| Basak03 | 2.7(1) | 3.9(0) | 22.9(1) | 21.6(1) | 11.0(2) | 12.8(2) |
| Cooper14 | 5.2(0) | 7.9(0) | 19.4(1) | 20.1(1) | 13.6(1) | 12.3(2) |
| Goel08 | 3.0(0) | 8.3(3) | 19.7(1) | 18.7(1) | 6.8(0) | 8.9(0) |
| Morelon03 | 5.8(1) | 9.0(1) | 17.0(1) | 16.6(0) | 8.6(0) | 10.2(2) |
| Read10 | 12.9(0) | 16.2(1) | 16.4(2) | 16.7(0) | 8.1(0) | 11.1(1) |
| Yakub10 | 3.8(0) | 5.4(0) | 18.7(1) | 18.0(1) | 11.1(2) | 12.7(2) |

**Table 3** Calculated Peierls stresses (in GPa) for the 1/2<110> edge and screw dislocations gliding on {100}, {110}, and {111}. Numbers in parentheses are uncertainties, related to small asymmetries in the underlying parameterization of the disregistry function, to which the absolute energy is relatively insensitive, but have a modest effect on the calculated Peierls stress. Values for the uncertainties are derived by applying both positive and negative stress to the dislocation, and calculating the Peierls stress in that direction
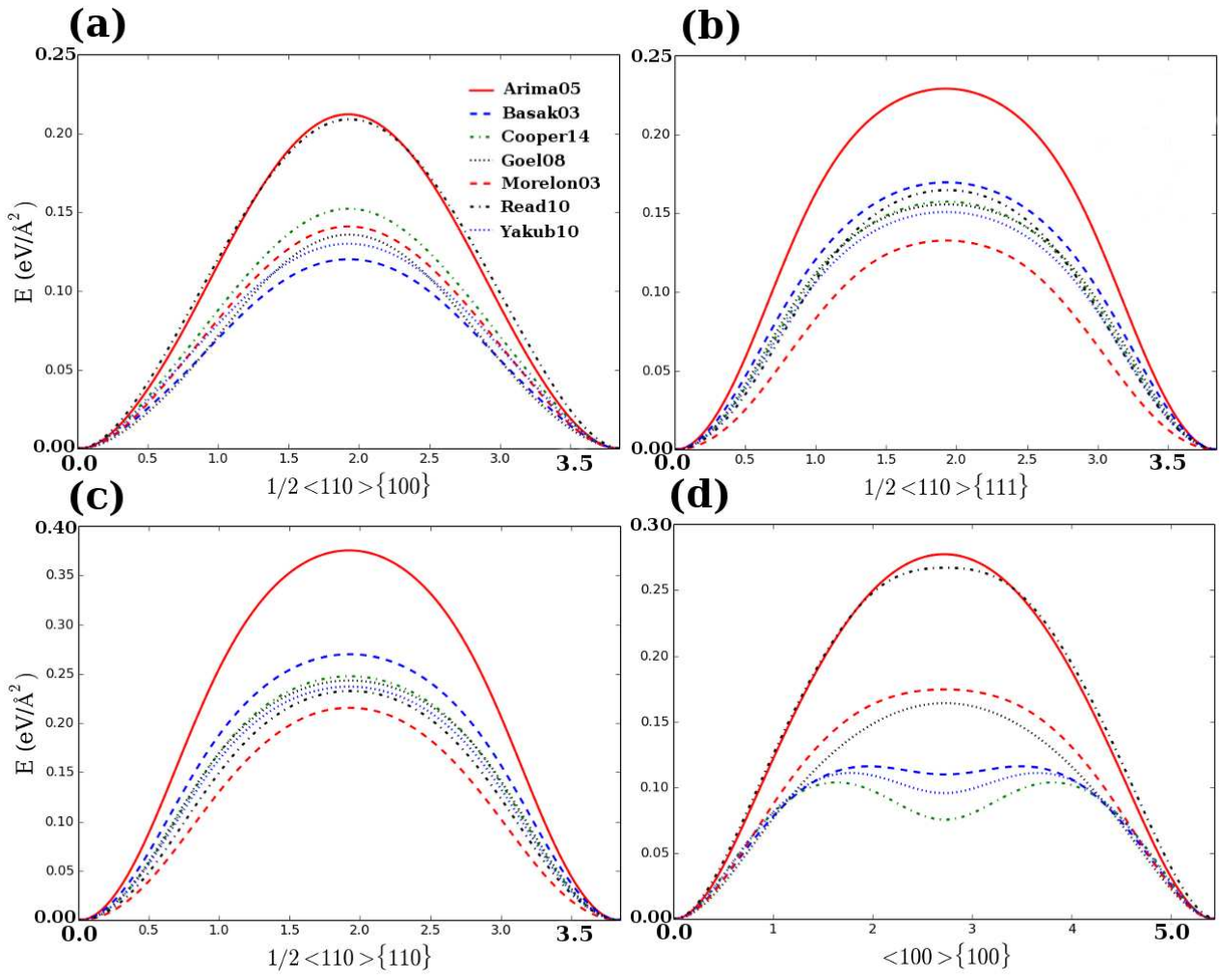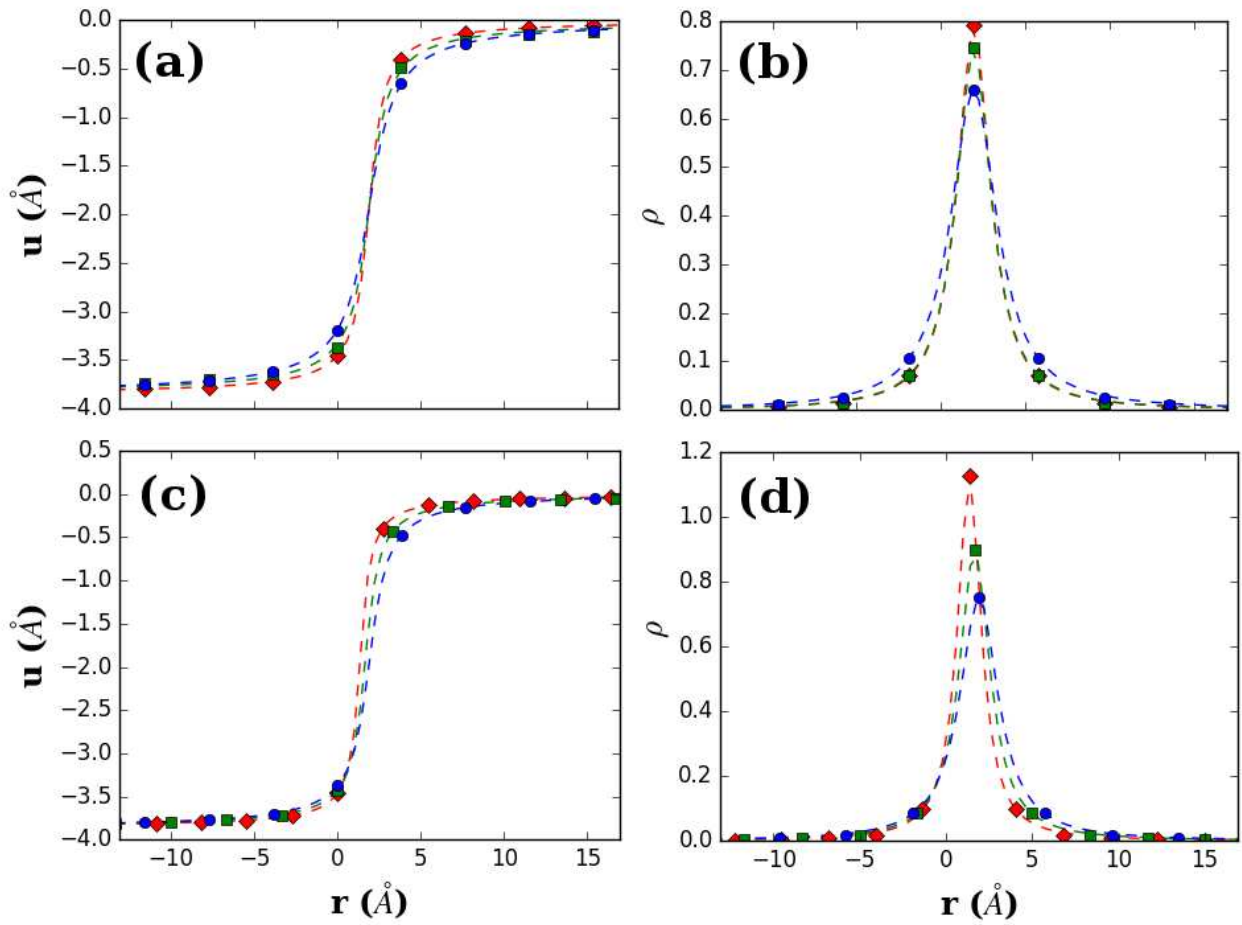
**Figures**
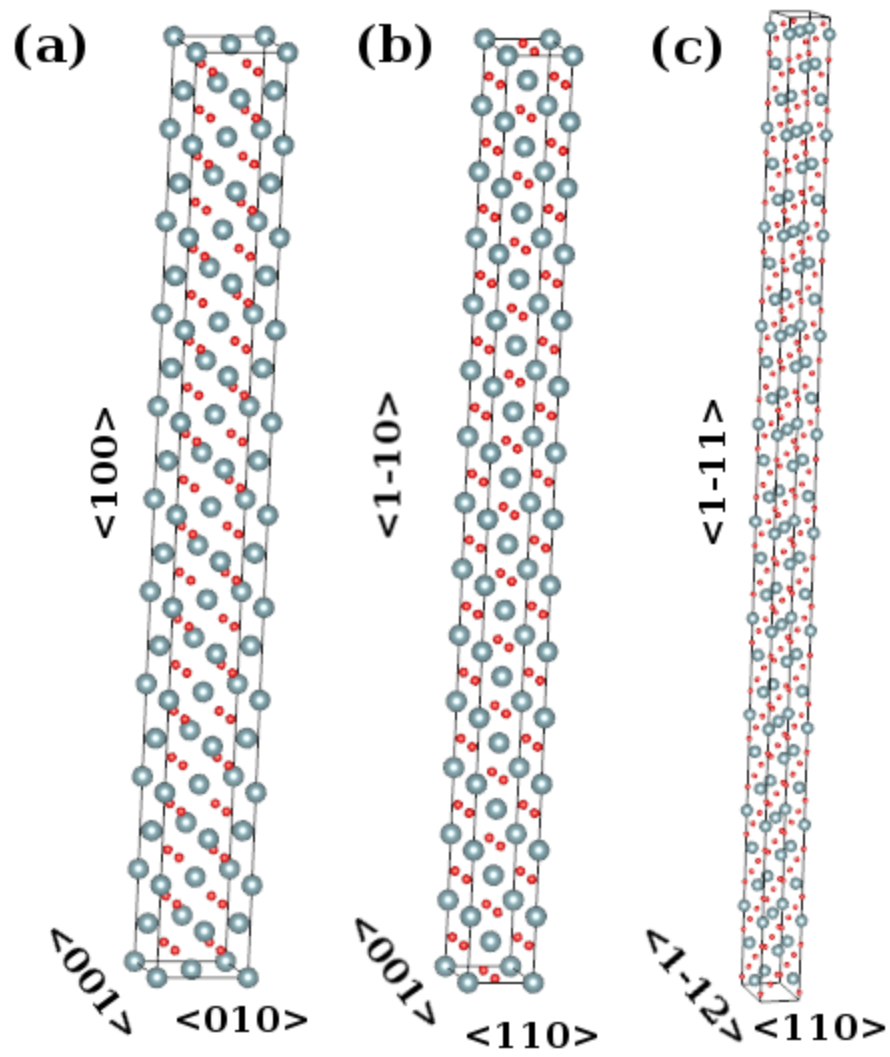


**Fig. 1.** Simulation cells used to calculate (a) {100}, (b) {110}, and (c) {111} γ-surface energies for UO₂.
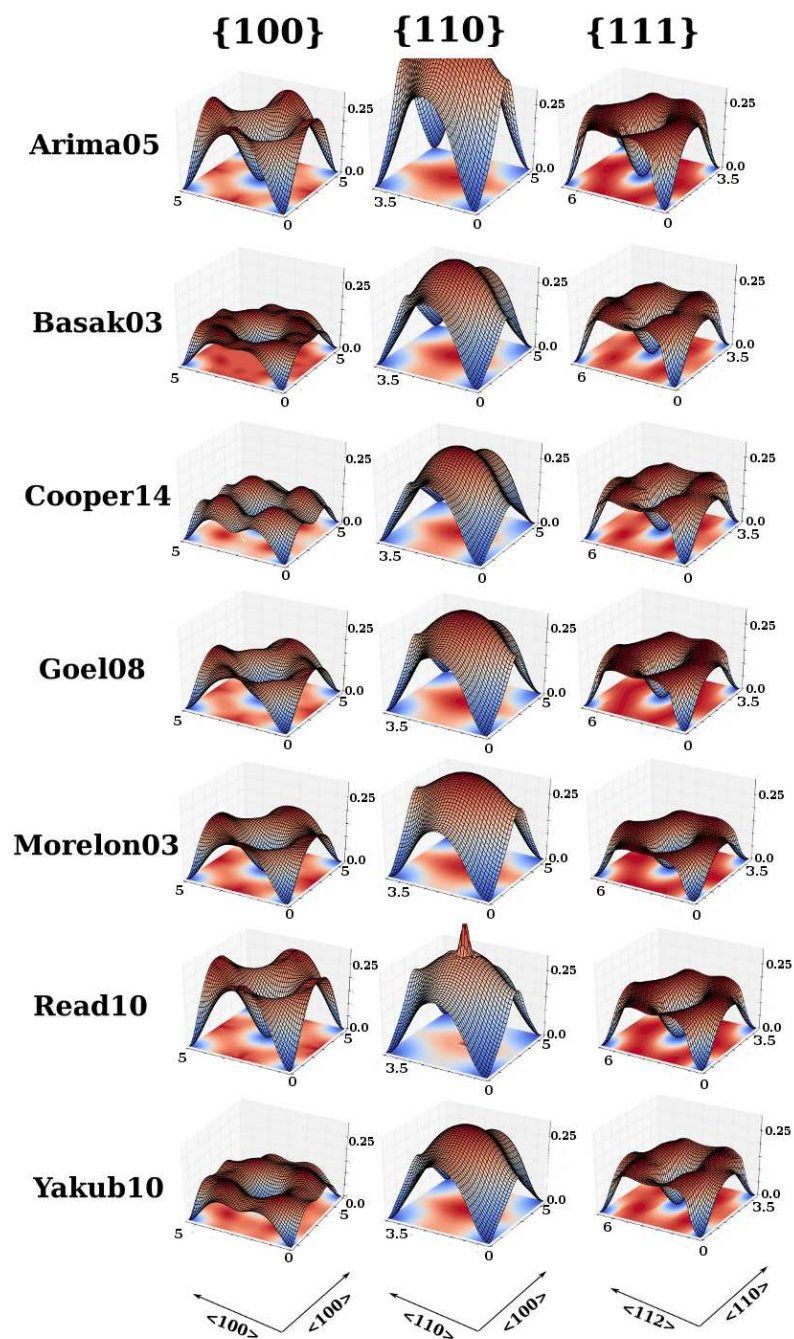
**Fig. 2.** Calculated {100}, {110}, and {111} γ-surfaces (in eV/Å) for the seven different interatomic potentials used in this study. For ease of comparison, all gamma surfaces have been plotted on the same energy scale.

**Fig. 3.** (a) 1/2<110>{100}, (b) 1/2<110>{111}, (c) 1/2<110>{110}, and (d) <100>{100} γ-lines for UO₂.

**Fig. 4.** (a) Misfit profiles for 1/2<110>{100} (circles), 1/2<110>{110} (diamonds), and 1/2<110> edge dislocations in UO2, calculated using the Cooper14 potential. (b) Misfit profiles calculated using the Cooper14 potential for 1/2<110> screw dislocations spreading on the {100 } (circles), {110} (diamonds), and {111} (squares) planes. The dislocation density distributions corresponding to these misfit profiles are plotted in (b) and (d) for the edge and screw dislocations, respectively.